Published in final edited form as:
ACS Chem Biol. 2012 January 20; 7(1): 210–217. doi:10.1021/cb200181v.

Towards Targeting RNA Structure: Branched Peptides as Cell Permeable Ligands to TAR RNA

David I. Bryson, **Wenyu Zhang**, **Patrick M. McLendon**, **Theresa M. Reineke**, and **Webster L. Santos***
Department of Chemistry, Virginia Tech, Blacksburg, VA 24061

Abstract

Rational design of RNA ligands continues to be a formidable challenge, but the potential powerful applications in biology and medicine catapults it to the forefront of chemical research. Indeed, small molecule and macromolecular intervention are attractive approaches but selectivity and cell permeability can be a hurdle. An alternative strategy is to use molecules of intermediate molecular weight that possess large enough surface area to maximize interaction with the RNA structure but are small enough to be cell permeable. Herein, we report the discovery of non-toxic and cell permeable branched peptide (BP) ligands that bind to TAR RNA in the low micromolar range from on-bead high throughput screening of 4,096 compounds. TAR is a short RNA motif in the 5′-UTR of HIV-1 that is responsible for efficient generation of full RNA transcripts. We demonstrate that BPs are selective for the native TAR RNA structure and that "branching" in peptides provides multivalent interaction, which increases binding affinity to RNA.

Introduction

RNA-protein interactions, along with protein-protein interactions, control many functions in a living cell such as transcription, splicing, replication, transport and catalysis. Owing to the ubiquity of RNA-mediated biological processes, molecules that can selectively bind and regulate the function of RNA have enormous potential application in biotechnology and therapeutics. Despite the considerable effort in utilizing RNA as a drug target, the discovery of molecules with desirable drug-like properties remains challenging and continues to be a subject of intense investigation (1). One of the main issues for RNA targeting is the involvement of large surface area for recognition and tight binding—outcompeting the endogenous protein partner using a small molecule is a herculean task. With RNA, the problem is exacerbated by the conformational dynamics often resulting in structural heterogeneity making it difficult for the *de novo* design of RNA ligands (2).

RNA is often characterized by a variety of secondary structures, including hairpins, bulges, stems, loops, pseudoknots, and turns. The folding of these local structures can give rise to tertiary structures that are unique to specific RNA constructs and potentially allow the RNA to be targeted selectively (3). The unique three dimensional architectures present in RNA make it possible to target at a level that is not presented by DNA and in a manner that is not solely dependent on Watson-Crick base pairing. For example, the ability of small molecules to target the tertiary structures of ribosomal RNA (rRNA) has been well demonstrated by aminoglycoside, macrolide, oxazolidinone, and tetracycline antibiotics (4–9). However, the development of RNA-binding small molecules is far from a straightforward process, where

santosw@vt.edu, phone: (540)231-5742.

Supporting Information Available: This material is available free of charge *via* the Internet at http://pubs.acs.org.

poor selectivity is a common hurdle to overcome, and a general RNA-targeting paradigm remains an elusive goal (1). The most desired approach of rational, structure-based RNA-targeted drug discovery is still in its infancy, making the design of RNA ligands difficult (10). RNA-targeted gene repression can be attained using antisense or RNA interference technologies (11). However, despite significant efforts from academia and the pharmaceutical industry, drug characteristics such as cellular delivery, stability and off-target effects remain a challenge, although several siRNAs are in clinical trials (11, 12).

The human immunodeficiency virus-1 (HIV-1) transactivation response element (TAR) is one of the most studied RNA targets because of its key role in viral replication (13). HIV-1 TAR is characterized by a 59-nucleotide stem-bulge-loop secondary structure, which is found at the 5′-end of all nascent HIV-1 transcripts and is a highly conserved region of the virus (14, 15). The region from +19 to +42 bases of HIV-1 TAR is characterized by a hexanucleotide loop at the end of a helical stem containing a single, trinucleotide pyrimidine bulge. HIV-1 TAR RNA is the target of the 101-amino acid Tat protein, which is the virally encoded *trans*-activator of HIV-1 transcription (14). When the Tat protein is not associated with HIV-1 TAR, basal viral transcription is very low, and short RNA transcripts are generated (16). When the Tat-TAR RNA complex is formed, cofactors such as cyclin T1 and its cognate kinase CDK9 stimulate efficient transcription from the long terminal repeat (LTR) (15). Blocking this Tat-TAR interaction is therefore a potent strategy for controlling the proliferation of the virus and provides a potential anti-HIV therapy.

Given the global problem of HIV-1 infection, drugs that exhibit novel modes of action are of the utmost importance since resistance to current HIV therapies has been observed (17). Indeed, the inhibition of Tat-TAR interaction can fill this gap. Notwithstanding the significant efforts committed to discovering compounds capable of disrupting the function of TAR, no drug has made it to the clinic. Several strategies have been reported to inhibit the Tat-TAR interaction. Although attractive, small molecules such as aminoglycosides, argininamide, purine analogs, bis-guanidine compounds, tripeptides and others appear to suffer from selectivity issues (1, 18–23). Large macromolecules such as TAR RNA decoys (24, 25) are currently being investigated, but compounds of intermediate size (oligomeric amines (26) and β-hairpin peptidomimetics (27, 28)) are subject to increased attention in part because of better overlap with the large surface area of RNA. In particular, cyclic peptide L50 has recently been shown to have anti-viral activity by inhibiting the tat dependent transcription process and the reverse transcription step (29).

While interesting leads are emerging from prior studies, molecular scaffolds that can recognize RNA structures still need to be developed. In an effort to provide a general platform to targeting RNA structures, we focused on inhibiting RNA-protein interactions involving Tat and TAR RNA (*vide supra*). Recently, we disclosed an approach that uses branched peptides (BPs) because of the potential for multivalent interaction on various regions of TAR—a desirable property that can increase selectivity and affinity (30). Because the TAR structure is expected to be a dynamic ensemble of many conformations in solution, high throughput screening of a library of BPs allows the highly populated TAR conformations to selectively bind compounds with diverse chemical architecture projected on beads. We reason that BPs are excellent candidates because natural and unnatural amino acids contain a wide array of functional groups that can display unique molecular architectures and their synthetic accessibility is straightforward. Indeed, rapid generation of a large number of peptides on beads using the split and pool technique can provide access to libraries of varying molecular weight that can be fine-tuned to increase pharmacological properties such as cell permeability. Herein, we report the discovery of BPs of intermediate molecular weight binding to TAR RNA in the low micromolar regime. In addition, we show that "branching" in peptides can lead to multivalent interactions that increase affinity to

TAR. Further, we demonstrate that BPs are cell permeable and non-toxic making them excellent chemical biology tools for targeting well-defined RNA structures and useful in anti-HIV drug discovery.

RESULTS and DISCUSSION

Design of branched peptides and on-bead high throughput screening

We recently reported the synthesis of a 4,096-membered BP library (30) on Tentagel beads by split and pool synthesis (20, 31–34). The amino acid composition of the library was biased to increase intermolecular interaction with RNA. For example in position 1, amino acids with functional groups that can induce attractive forces such as electrostatics (the positively charged Arg interacting with the negatively charged phosphate backbone), π-π interactions (Tyr) and hydrogen bonding (Asp, His) were introduced (Figure 1). Presentation of diverse epitopes on the bead surface would allow DY547-labeled TAR RNA to sample all possible binding modes. Binding of the RNA to the bead resulted in increased fluorescence, which was monitored by confocal microscopy. The BPs in the screened library featured two identical N-termini branched by a Lys residue and a single C-terminus, which was linked to the bead *via* a photocleavable linker (3-amino-3-(2-nitrophenyl)propionic acid, ANP) (35). During the incubation, nonspecific binding was minimized with the addition of excess unlabeled alpha-synuclein mRNA (340-nt) and BSA in the incubation buffer. Seventeen beads were selected as putative hits, photocleaved and identified by matrix assisted laser desorption ionization time-of-flight (MALDI-TOF) *de novo* sequencing (36).

Synthesis of Fluorescein-labeled Branched Peptides and Truncated Variants

The BPs were synthesized following standard solid-phase peptide synthesis techniques using Rink Amide MBHA resin. Each BP was prepared such that a single N-terminus was labeled with fluorescein using fluorescein isothiocyanate (FITC, Scheme 1). The branching unit was attached to the ε-nitrogen of Lys that was orthogonally protected with ivDde; therefore, although the two branches were similar, the spacing was different. Over the course of this study, we found that directly coupling the N-terminal amino acid to FITC resulted in poor isolated yields after HPLC purification. Upon further analysis of the crude peptides, we observed a strong signal in the MALDI-TOF mass spectrum corresponding to truncated peptide, where fluorescein and the adjacent amino acid were cleaved. This result suggested that acid mediated formation of fluorescein thiohydantoins was occurring upon cleavage from solid-support resin with trifluoroacetic acid (TFA) (37). Installation of aminohexanoic acid (Ahx) as spacer between the N-terminal amino acid and fluorescein resolved the problematic autocleavage and resulted in increased overall yield. Further, one particular peptide, **FL15**, epimerized resulting in two diastereomers of equal intensity that were separated by HPLC and confirmed by LC-ESI/MS (see supporting information). **FL15** was finally prepared as the single diastereomer by using [ethyl cyano(hydroxyimino)acetato-O^2]tri-1-pyrrolidinylphosphonium hexafluorophosphate (PyOxim) as coupling reagent.

Binding Affinities of Hit Branched Peptides to HIV-1 TAR

Consensus sequence analysis of BP hits from the HTS revealed seventeen peptide sequences that appear to have a preference for Arg moieties. This result is not surprising due to the strong electrostatic attraction between the positively charged side chain of the peptides and the negatively charged phosphate backbone of the RNA target. To validate binding of BP hits to TAR RNA and eliminate false positives, dissociation constants (K_d values) were measured using dot blot assay (Table 1). Our results indicate binding affinities in the low micromolar range, with one peptide hit (**FL10**) determined as a false positive. In particular, **FL4**, **FL6** and **FL7** contained four positively charged Arg residues in the N-termini and had K_d values of 600 nM, 1.2 μM and 1.2 μM, respectively. Gratifyingly, **FL4** bound much

tighter than its native protein counterpart, Tat (K_d = 780 nM). The sequence of **FL4** ($[RRW]_2$*HAL) was different from **FL7** in that the last 2 amino acid residues were changed to YD—the slight decrease (2 fold) in binding affinity might be as a result of the presence of an anionic Asp residue that imparts repulsive interaction with the phosphate backbone of TAR. Surprisingly, the additional Arg moiety in **FL6** did not result in increased binding affinity but suggested that a putative electrostatic interaction with a positive charge could be compensated with other modes of interaction. **FL12** was nearly identical in sequence with **FL4** except for the Leu→Ser change; the switch from hydrophobic to hydrophilic group resulted in a 3-fold decrease in binding affinity. In general, however, a hydrophobic moiety was desired in amino acid position 6 since hydrophobic groups in this position tended to have higher binding affinity for TAR (Table 1).

From the pool of seventeen BPs, three peptides (**FL2**, **FL3** & **FL8**) did not contain the consensus Arg-Arg in the N-termini. These peptides had similar dissociation constants at around 8 μM. Compounding the elevation in K_d relative to **FL4** was the corresponding decrease in solubility in aqueous condition—DMSO was added to the buffer used in the dotblot assay—that may contribute to decrease in affinity. Finally, it is noteworthy that the electrostatic interaction mediated by the two Arg moieties in the N-termini did not contribute to the majority of the binding affinity with TAR since **FL13** and **FL15** had K_d values > 75 μM.

The Branched N-terminus Imparts Multivalency

To determine whether the additional “branch” in our peptides results in complementary increase in binding affinity as a consequence of multivalency, we synthesized **T4-1** as a truncated variant of the strongest binder, **FL4. T4-1** (RRWGHAL) featured a single N-terminus and a C-terminus that were identical to **FL4**. We substituted the branching Lys unit with Gly in **T4-1** to preserve the spacing between the N- and C-termini, and to avoid incorporating any additional functionality compared to **FL4**. To our delight, we observed a > 125-fold decrease in binding affinity for **T4-1** (K_d > 75 μM) compared to **FL4** when measured by dot blot assay (Table 1). While it is tempting to draw a conclusion that **T4-1** displayed such a dramatic loss of affinity because two positively charged side-chains were omitted, the presence of Arg-Arg in the N-termini did not necessarily result in effective RNA binding (*vide supra*). We also note that the decrease in binding affinity was not a result of the decrease in the number of positive charges in the molecule because BPs with five positive charges (**FL5**, **FL6**, **FL15**, and **FL17**) had lower K_d values. These results suggest that electrostatic interactions were not solely responsible for high affinity binders but that all branches of the 3.3.3 peptide were responsible for tight binding with the RNA. This conclusion is intriguing because a central problem with designing RNA binding molecules is that inclusion of multiple positive charges generally increases affinity, but a significant price is paid in the reduced selectivity of such compounds (26). Thus, it stands to reason that the incorporation of diverse binding interactions in RNA targeting molecules will prove to be an important feature when designing effective binders that attain high selectivity.

Selectivity Determination and Identification of Requisite TAR Binding Elements

In order to interrogate the selectivity of **FL4**, dot blots were performed in the presence of excess tRNA and a series of modified TAR RNA structures. First, we confirmed that the dissociation constants determined from the dot blot assay were reliable by performing electrophoretic mobility shift assay (EMSA) with **FL4** (see supporting information). As shown in Figure 2, the dissociation constant determined through EMSA was in excellent agreement with the dot blot data (0.5 ± 0.1 μM and 0.6 ± 0.1 μM, respectively). Consistent with previous reports using EMSA, we also noticed non-specific binding to TAR RNA in the presence and absence of competitor tRNA (see supporting information) (26, 39).

Addition of 10- and 1000-fold excess of tRNA caused a shift in the binding affinity to ^{32}P-labeled TAR RNA suggesting that **FL4** was partially selective.

In order to determine the selectivity of **FL4** with the native TAR RNA structure, we synthesized TAR sequences containing a point mutation (24U>C), bulgeless TAR, tetraloop TAR, and bulgeless tetraloop TAR (Figure 3A). The measured K_d using TAR (24U>C) on the 3-nt bulge, a site where tat is known to bind, was 0.8 ± 0.2 μM (Figure 3B). This value is within experimental error of the native TAR K_d in this assay and suggests that **FL4** may not directly interact with the nucleobase in U or C. Indeed, TAR (24U>C) is a mutation that is present in several clades of HIV-1 and is expected to retain the native structure of TAR (26) (40). In contrast, a more dramatic increase in K_d was observed when the TAR RNA tertiary structure was modified as a consequence of removing the 3-nt bulge region (bulgeless TAR) or decreasing the size of the apical loop region by 2-nt (tetraloop TAR). The resulting K_d for these TAR variants were 6.6 ± 1.3 μM and 5.5 ± 2.0 μM, respectively (Figure 3B). The approximately ten-fold decrease in binding affinity is exciting because it suggests that **FL4** is selective for the three dimensional structure of native TAR RNA and that **FL4** may interact with both of these structural elements when bound to the native TAR RNA.

We anticipated that modifying both structural elements simultaneously (bulgeless tetraloop TAR) would further decrease the binding affinity if **FL4** indeed spans the bulge and apical loop of TAR RNA. However, implementing both modifications resulted in a K_d value of 3.5 ± 1.0 μM, which was within error of tetraloop TAR. It is possible that the additional decrease in affinity is not observed with bulgeless tetraloop TAR because the tertiary structure is sufficiently altered to preclude **FL4** from binding. The Hill analyses of our dot blot data for native TAR RNA and TAR (24U>C) yield Hill coefficients (n) of 1.4 and 1.2 (see supporting information), respectively, suggesting non-cooperative binding of **FL4**, where n is near 1. This supports our hypothesis of a single binding site that spans the bulge and apical loop, as the binding affinity is clearly decreased when these structural elements are removed individually. Furthermore, cooperative binding ($n \geq 1.5$) is observed for bulgeless TAR, tetraloop TAR and bulgeless tetraloop TAR, which presented Hill coefficients of 1.5, 2.1, and 1.6 respectively. Taken together, these results suggest that modifications on TAR result in multiple, low-affinity binding sites for **FL4**.

Branched Peptides are cell permeable and exhibit no cytotoxicity

An attractive feature of developing BPs as RNA ligands is the ability to control the molecular weight, a property that can have significant influence on cellular uptake. Although arginine-rich BPs (Arg > 8) have been shown to be cell permeable (41), the spacing and number of Arg residues present in our BP hits are significantly different than previously reported examples. We biased our investigation to 3.3.3-BP in part because of their medium molecular weight (*i.e.*, larger than 500 Da but less than typical oligonucleotides/peptide nucleic acids), which is around 1400 Da. Based on the hit sequences revealed through HTS, we predicted that our BPs would be cell permeable due to the high content of basic residues and because they were less than 20-amino acids in size (42–45). Cellular uptake in HeLa cells was determined upon incubation with FITC-labeled BPs (1 μM) in the culture medium for 4 hours at 37 °C. After washing, cells were fixed with 4% paraformaldehyde and imaged using a confocal microscope. Cells incubated with **FL3** contained fluorescence that was diffuse throughout the nucleus and cytoplasm (Figure 4A). Punctate structures were also observed in cells incubated with other BPs, wherein BPs were suspected to be internalized *via* endocytosis and sequestered in vesicles (see supporting information). Flow cytometry studies with HeLa cells also provided supporting evidence that BPs were cell permeable (Figure 4B). Gratifyingly, the majority of the peptides were internalized by >95% of the counted cells; although **FL9**, **FL15** and **FL16** showed a lesser degree of internalization (~20–55% increased fluorescence compared to background). To

our delight, the majority of cells were viable in an MTT assay suggesting that BPs that penetrate cells were nontoxic (Figure 4C). Overall, medium-sized BPs were cell permeable and demonstrated low cytotoxicity.

Conclusion

In summary, a general platform for generating selective RNA-binding ligands based on multivalent, branched peptides has been developed. In targeting the Tat-TAR RNA interaction, non-toxic and cell permeable compounds binding to the RNA component in the low micromolar regime were discovered. Selective binding of branched peptide **FL4** to the tertiary structure of TAR RNA against other variants was demonstrated, where a single binding site that spans the bulge and apical loop is likely involved. Targeted localization of BP in specialized regions of the cell can be important in realizing their therapeutic potential in various disease states such as HIV-1. Current efforts are aimed at introducing localization signal modules that can deliver BPs into the nucleus. The selective targeting of RNA structures remains a formidable task; the current effort steps towards the realization of a possible solution.

METHODS

Peptide Synthesis, Purification, and Characterization

All reagents were purchased from Novabiochem unless stated otherwise. N-α-Fmoc protected L-amino acids (3 equiv.) were used at all steps except when Fmoc-Lys(ivDde)-OH was used as the branching unit in the BPs. All coupling steps were 15 minutes at room temperature and performed in dimethylformamide (DMF) bubbling with argon. Deprotection of Fmoc was performed with two consecutive 5 minute washes with 20% piperidine in DMF. Peptides were synthesized on Rink amide MBHA resin (100–200 mesh) by hand using the previously described apparatus (30). 2-(6-chloro-1-H-benzotriazole-1-yl)-1,1,3,3-tetramethylaminiumhexafluorophosphate (HCTU) (Peptides International) was used as coupling reagent (3 equiv.) and N, N-diisopropylethylamine as base (5 equiv.) in all coupling steps except for the preparation of **FL15**, where PyOxim (3 equiv.) was required as the coupling reagent to avoid epimerization in the sequence. Acetic anhydride (3 equiv.) was used to cap the first N-terminus in all BPs using DIEA (5 equiv.) as base. The ivDde protecting group was then removed using 2% hydrazine in DMF, and the second N-terminus was synthesized off of the Lys side-chain in the BPs. Fmoc-6-Ahx-OH (AnaSpec) was installed at the uncapped N-terminus in the samples used in dot blot and EMSA experiments. Fluorescein 5-isothiocyanate (FITC) (Sigma) (5 equiv) was coupled last to the uncapped N-terminus of all peptides using DIEA (14 equiv) as base (3 hours). Peptides were protected from the light at all subsequent steps. Side chains were deprotected and peptides cleaved from resin simultaneously by stirring for 3 hours in a 95:2.5:2.5 (v/v/v) mixture of trifluoroacetic acid (TFA):water:triisopropylsilane. The supernatant was dried under reduced pressure, and the crude peptide was washed with cold diethyl ether. Peptides were purified to ≥95% purity by HPLC (Agilent 1200 series) using a Jupiter 4 μ Proteo 90 Å semi-prep column (Phenomenex), and a binary solvent gradient composed of 0.1% TFA in MilliQ water and HPLC grade acetonitrile. Purity was determined under the same conditions using a Jupiter 4 μ Proteo 90 Å analytical column (Phenomenex). All peptides were finally characterized by MALDI-TOF MS analysis. Peptide stock concentrations were prepared by spectrophotometry, by monitoring absorbance of FITC at 495 nm, $\varepsilon = 77{,}000\ mol^{-1}cm^{-1}$ in 100 mM glycine, pH 9.0.

Cellular Internalization of Peptides

HeLa cells were plated at 1×10^5 cells/well in DMEM containing 10% FBS in 12-well tissue culture plates (Corning) and allowed to attach at 37 °C in a humid 5% CO_2

atmosphere for 24 hours. After removing media and washing cells with PBS, 600 μl of FITC-labeled peptide in Opti-MEM (1 μM) was added to each well. Cells were incubated with peptides for 4 hours, then 1.5 ml DMEM was added and incubated for 30 minutes. Cells were detached with 500 μL of trypsin-EDTA, quenched with internalization media (1 mL), and the contents of each well were collected into Falcon Tubes (BD Biosciences). Cells were centrifuged at 4 °C and 1250 rpm for 10 minutes. The supernatant was removed and the cell pellets rinsed with PBS, and centrifuged again at identical conditions. Supernatant was removed and cell pellet was again suspended in 2% FBS in PBS. Propidium iodide (PI; 5 μg ml^{-1}, Molecular probes) was added to each tube 2–5 minutes prior to analysis. Cellular uptake of FITC–labeled peptides was measured on a FACS Canto II flow cytometer (BD Biosciences). FITC was excited using a 488 nm solid state laser, and detected at 530 ± 30 nm bandpass filter, and PI was excited using a 488 nm solid state laser and detected with a 670 nm longpass filter. Appropriate gating was done against the untreated cells control to ensure that autofluorescence was not measured as cellular uptake, and only live (PI-negative) cells were included in subsequent analysis. 10,000–20,000 gated events were collected for each sample, and experiments were done in duplicate unless noted otherwise.

Preparation of ^{32}P-Labeled RNA

RNA was prepared by *in vitro* transcription with the Ribomax T7 Express System (Promega) using previously reported techniques (46). All steps were done using RNase free conditions. The antisense template and sense complementary strand, 5′-ATGTAATACGACTCACTATAGG (Integrated DNA Technologies), were annealed prior to transcription by heating an equimolar mixture of the ssDNA strands in water at 65 °C for 2 minutes followed by a 2 minute incubation in an ice bath. Antisense template sequences used were as follows: HIV-1 TAR, 5′-GCCCGAGAGCTCCCAGGCTCAAATCGGGCCTATAGTGAGTCGTATTACAT; TAR(24U>C), 5′-GCCCGAGAGCTCCCAGGCTCATATCGGGCCTATAGTGAGTCGTATTACAT; bulgeless TAR, 5′-GCCCGAGAGCTCCCAGGCTCTCGGGCCTATAGTGAGTCGTATTACAT; tetraloop TAR 5′-GCCCGAGAGCCGAAGCTCAAATCGGGCCTATAGTGAGTCGTATTACAT; bulgeless tetraloop TAR, 5’-GCCCGAGAGCCGAAGCTCTCGGGCCTATAGTGAGTCGTATTACAT. After transcription, the DNA was degraded by DNase. The newly transcribed HIV-1 TAR RNA was purified by 20% denaturing PAGE. The topmost band was excised and eluted from the gel overnight in 300 mM sodium acetate, 10 mM Tris•HCl, pH 7.4, and 10 mM EDTA. The sample was desalted using a NAP-25 column (GE Healthcare) and lyophilized to dryness before treating with calf intestinal phosphatase in NEBuffer 3 (New England BioLabs). The dephosphorylated RNA was recovered by phenol extraction followed by ethanol precipitation. Preparation of the full-length transcript was confirmed by MALDI-TOF. Dephosphorylated RNA was stored as a pellet at −80 °C.

HIV-1 TAR RNA was labeled at the 5′-end by treating 100 pmoles of dephosphorylated RNA with 20 nmoles of [γ-^{32}P]ATP (111 TBq mol^{-1}) and 20 units of T4 polynucleotide kinase in 70 mM Tris•HCl, pH 7.6, 10 mM $MgCl_2$, and 5 mM dithiothreitol. The mixture was incubated at 37 °C for 1 hour followed by a 10 minute incubation at 65 °C. The labeled RNA was recovered by ethanol precipitation. A 20% denaturing PAGE run at 25W for 2.25 hours followed by autoradiography was used to ensure that the RNA sample was ≥95% pure prior to use in EMSA and dot blot assays. The ^{32}P-labeled RNA was stored at a concentration of 500 nM in water at −20 °C for up to two months without measurable degradation.

Dot Blot Assay

Dot blot assays were performed in triplicate using a Whatman Minifold I 96 well Dot Blot system and Whatman 0.45 μm pore size Protran nitrocellulose membranes. Assays were carried out by first refolding 800 pM ^{32}P-labeled HIV-1 TAR RNA in 2X TK buffer (100 mM Tris•HCl, pH 7.4, and 200 mM KCl) by heating the sample at 95 °C for three minutes and then allowing it to cool slowly at room temperature for 20 minutes. Peptides were diluted with water or 10% DMSO from 200 μM stocks to prepare each series at 2X concentrations ranging from 0.002 μM to 200 μM at half-log intervals. 25 μL aliquots of refolded ^{32}P-labeled HIV-1 TAR RNA in 2X TK buffer were added to 25 μL aliquots of the peptides at 2X concentration to give the desired final concentration of each component. The mixtures incubated at room temperature for 20 minutes prior to filtering each 50 μL sample through the nitrocellulose membrane, which had been pre-equilibrated in 1X TK buffer. Two consecutive 50 μL washes with 1X TK buffer followed each filtration. Peptide binding was measured by autoradiography using a storage phosphor screen (GE Healthcare), which was imaged on a Typhoon Trio (GE Health Care). Densitometry measurements were taken in ImageQuant TL (Amersham Biosciences). Binding curves were generated using Kaleidagraph (Synergy Software). Error bars represent the standard deviation calculated for three replicates.

EMSA

EMSA assays were performed in duplicate by first refolding 4 nM ^{32}P-labeled HIV-1 TAR RNA in 2X TK buffer (100 mM Tris•HCl, pH 7.4, and 200 mM KCl) using the previously described method (*vide supra*). Peptides were diluted with water from 200 μM stocks to prepare each series at 2X concentration. 10 μL aliquots of refolded ^{32}P-labeled HIV-1 TAR RNA in 2X TK buffer were added to 10 μL aliquots of the peptides at 2X concentration to give the desired final concentration of each component. The mixtures incubated at room temperature for 20 minutes followed by the addition of 2 μL of 30% glycerol for loading. 15 μL of each sample was loaded on to a 10% native PAGE, which had pre-run for 1 hour at 300 V. The samples electrophoresed for 1 hour at 300 V. Gels were dried to filter paper prior to autoradiography. Data was measured as the percentage of bound RNA in each lane and error bars represent the standard deviation calculated for two replicates. Selectivity studies were performed in the presence of 10-fold excess by mass of tRNA from E.Coli MRE 600 (Roche). The tRNA was refolded separately from HIV-1 TAR RNA prior to use.

Supplementary Material

Refer to Web version on PubMed Central for supplementary material.

Acknowledgments

We thank K. Ray and R. Helm in the VT mass spectrometry incubator for their assistance with sequencing and M. Congdon and M. Paye for peptide synthesis and analysis. This work was supported by VT Chemistry department, Institute for Critical Technology and Applied Science, Macromolecular Interfaces with Life Science (NSF-IGERT DGE-0333378) and NIH (RO1 GM093834).

References

1. Thomas JR, Hergenrother PJ. Targeting RNA with small molecules. Chem Rev. 2008; 108:1171–1224. [PubMed: 18361529]
2. Lu J, Kadakkuzha BM, Zhao L, Fan M, Qi X, Xia T. Dynamic ensemble view of the conformational landscape of HIV-1 TAR RNA and allosteric recognition. Biochemistry. 2011; 50:5042–5057. [PubMed: 21553929]

3. Zaman GJR, Michiels PJA, van Boeckel CAA. Targeting RNA: new opportunities to address drugless targets. Drug Discov Today. 2003; 8:297–306. [PubMed: 12654542]
4. Carter AP, Clemons WM, Brodersen DE, Morgan-Warren RJ, Wimberly BT, Ramakrishnan V. Functional insights from the structure of the 30S ribosomal subunit and its interactions with antibiotics. Nature. 2000; 407:340–348. [PubMed: 11014183]
5. Tor Y. The ribosomal A-site as an inspiration for the design of RNA binders. Biochimie. 2006; 88:1045–1051. [PubMed: 16581175]
6. Brodersen DE, Clemons WM Jr, Carter AP, Morgan-Warren RJ, Wimberly BT, Ramakrishnan V. The Structural Basis for the Action of the Antibiotics Tetracycline, Pactamycin, and Hygromycin B on the 30S Ribosomal Subunit. Cell. 2000; 103:1143–1154. [PubMed: 11163189]
7. Wilson DN, Harms JM, Nierhaus KH, Schlünzen F, Fucini P. Species-specific antibiotic-ribosome interactions: implications for drug development. Biol Chem. 2005; 386:1239–1252. [PubMed: 16336118]
8. Hermann T. Drugs targeting the ribosome. Curr Opin Struct Biol. 2005; 15:355–366. [PubMed: 15919197]
9. Leach KL, Swaney SM, Colca JR, McDonald WG, Blinn JR, Thomasco Lisa M, Gadwood RC, Shinabarger D, Xiong L, Mankin AS. The Site of Action of Oxazolidinone Antibiotics in Living Bacteria and in Human Mitochondria. Mol Cell. 2007; 26:393–402. [PubMed: 17499045]
10. Lee MM, Pushechnikov A, Disney MD. Rational and Modular Design of Potent Ligands Targeting the RNA That Causes Myotonic Dystrophy 2. ACS Chem Biol. 2009; 4:345–355. [PubMed: 19348464]
11. Davidson BL, McCray PB. Current prospects for RNA interference-based therapies. Nat Rev Genet. 2011; 12:329–340. [PubMed: 21499294]
12. Watts JK, Corey DR. Clinical status of duplex RNA. Bioorg Med Chem Lett. 2010; 20:3203–3207. [PubMed: 20399650]
13. Stevens M, De Clercq E, Balzarini J. The regulation of HIV-1 transcription: molecular targets for chemotherapeutic intervention. Med Res Rev. 2006; 26:595–625. [PubMed: 16838299]
14. Rana TM, Jeang KT. Biochemical and Functional Interactions between HIV-1 Tat Protein and TAR RNA. Arch Biochem Biophys. 1999; 365:175–185. [PubMed: 10328810]
15. Bannwarth S, Gatignol A. HIV-1 TAR RNA: The Target of Molecular Interactions Between the Virus and its Host. Cur HIV Res. 2005; 3:61–71.
16. Keen NJ, Gait MJ, Karn J. Human immunodeficiency virus type-1 Tat is an integral component of the activated transcription-elongation complex. Proc Natl Acad Sci U S A. 1996; 93:2505–2510. [PubMed: 8637904]
17. Hirsch MS, Brun-Vézinet F, Clotet B, Conway B, Kuritzkes DR, D'Aquila RT, Demeter LM, Hammer SM, Johnson VA, Loveday C, Mellors JW, Jacobsen DM, Richman DD. Antiretroviral Drug Resistance Testing in Adults Infected with Human Immunodeficiency Virus Type 1: 2003 Recommendations of an International AIDS Society-USA Panel. Clin Infect Dis. 2003; 37:113–128. [PubMed: 12830416]
18. Tao J, Frankel AD. Specific binding of arginine to TAR RNA. Proc Natl Acad Sci U S A. 1992; 89:2723–2726. [PubMed: 1557378]
19. Pang R, Zhang C, Yuan D, Yang M. Design and SAR of new substituted purines bearing aryl groups at N9 position as HIV-1 Tat-TAR interaction inhibitors. Biorg Med Chem. 2008; 16:8178–8186.
20. Hwang S, Tamilarasu N, Ryan K, Huq I, Richter S, Still WC, Rana TM. Inhibition of gene expression in human cells through small molecule-RNA interactions. Proc Natl Acad Sci U S A. 1999; 96:12997–13002. [PubMed: 10557261]
21. Mei HY, Mack DP, Galan AA, Halim NS, Heldsinger A, Loo JA, Moreland DW, Sannes-Lowery KA, Sharmeen L, Truong HN, Czarnik AW. Discovery of selective, small-molecule inhibitors of RNA complexes--I. The Tat protein/TAR RNA complexes required for HIV-1 transcription. Bioorg Med Chem. 1997; 5:1173–1184. [PubMed: 9222511]
22. Davis B, Afshar M, Varani G, Murchie AI, Karn J, Lentzen G, Drysdale M, Bower J, Potter AJ, Starkey ID, Swarbrick T, Aboul-ela F. Rational design of inhibitors of HIV-1 TAR RNA through the stabilisation of electrostatic "hot spots". J Mol Biol. 2004; 336:343–356. [PubMed: 14757049]

23. Murchie AI, Davis B, Isel C, Afshar M, Drysdale MJ, Bower J, Potter AJ, Starkey ID, Swarbrick TM, Mirza S, Prescott CD, Vaglio P, Aboul-ela F, Karn J. Structure-based drug design targeting an inactive RNA conformation: exploiting the flexibility of HIV-1 TAR RNA. J Mol Biol. 2004; 336:625–638. [PubMed: 15095977]
24. Michienzi A, Li S, Zaia JA, Rossi JJ. A nucleolar TAR decoy inhibitor of HIV-1 replication. Proc Natl Acad Sci U S A. 2002; 99:14047–14052. [PubMed: 12376617]
25. Bohjanen PR, Colvin RA, Puttaraju M, Been MD, GarciaBlanco MA. A small circular TAR RNA decoy specifically inhibits Tat-activated HIV-1 transcription. Nucleic Acids Res. 1996; 24:3733–3738. [PubMed: 8871552]
26. Wang D, Iera J, Baker H, Hogan P, Ptak R, Yang L, Hartman T, Buckheit RW Jr, Desjardins A, Yang A, Legault P, Yedavalli V, Jeang KT, Appella DH. Multivalent binding oligomers inhibit HIV Tat-TAR interaction critical for viral replication. Bioorg Med Chem Lett. 2009; 19:6893–6897. [PubMed: 19896372]
27. Davidson A, Leeper TC, Athanassiou Z, Patora-Komisarska K, Karn J, Robinson JA, Varani G. Simultaneous recognition of HIV-1 TAR RNA bulge and loop sequences by cyclic peptide mimics of Tat protein. Proc Natl Acad Sci U S A. 2009; 106:11931–11936. [PubMed: 19584251]
28. Athanassiou Z, Patora K, Dias RL, Moehle K, Robinson JA, Varani G. Structure-guided peptidomimetic design leads to nanomolar beta-hairpin inhibitors of the Tat-TAR interaction of bovine immunodeficiency virus. Biochemistry. 2007; 46:741–751. [PubMed: 17223695]
29. Lalonde MS, Lobritz MA, Ratcliff A, Chamanian M, Athanassiou Z, Tyagi M, Wong J, Robinson JA, Karn J, Varani G, Arts EJ. Inhibition of both HIV-1 reverse transcription and gene expression by a cyclic peptide that binds the Tat-transactivating response element (TAR) RNA. PLoS pathogens. 2011; 7:e1002038. [PubMed: 21625572]
30. Bryson DI, Zhang W, Ray WK, Santos WL. Screening of a Branched Peptide Library with HIV-1 TAR RNA. Mol BioSyst. 2009; 5:1070–1073. [PubMed: 19668873]
31. McNaughton BR, Gareiss PC, Miller BL. Identification of a Selective Small-Molecule Ligand for HIV-1 Frameshift-Inducing Stem-Loop RNA from an 11,325 Member Resin Bound Dynamic Combinatorial Library. J Am Chem Soc. 2007; 129:11306–11307. [PubMed: 17722919]
32. Furka A, Sebestyen F, Asgedom M, Dibo G. General method for rapid synthesis of multicomponent peptide mixtures. Int J Pept Protein Res. 1991; 37:487–493. [PubMed: 1917305]
33. Lam KS, Salmon SE, Hersh EM, Hruby VJ, Kazmierski WM, Knapp RJ. A new type of synthetic peptide library for identifying ligand-binding activity. Nature. 1991; 354:82–84. [PubMed: 1944576]
34. Lescrinier T, Hendrix C, Kerremans L, Rozenski J, Link A, Samyn B, Aerschot AV, Lescrinier E, Eritja R, Beeumen JV, Herdewijn P. DNA-Binding Ligands from Peptide Libraries Containing Unnatural Amino Acids. Chem Eur J. 1998; 4:425–433.
35. Brown BB, Wagner DS, Geysen HM. A single-bead decode strategy using electrospray ionization mass spectrometry and a new photolabile linker: 3-amino-3-(2-nitrophenyl)propionic acid. Mol Divers. 1995; 1:4–12. [PubMed: 9237189]
36. Crumpton JB, Zhang W, Santos WL. Facile Analysis and Sequencing of Linear and Branched Peptide Boronic Acids by MALDI Mass Spectrometry. Anal Chem. 2011; 83:3548–3554. [PubMed: 21449540]
37. Jullian M, Hernandez A, Maurras A, Puget K, Amblard M, Martinez J, Subra G. N-terminus FITC labeling of peptides on solid support: the truth behind the spacer. Tetrahedron Lett. 2009; 50:260–263.
38. Wang X, Huq I, Rana TM. HIV-1 TAR RNA Recognition by an Unnatural Biopolymer. J Am Chem Soc. 1997; 119:6444–6445.
39. Gelman MA, Richter S, Cao H, Umezawa N, Gellman SH, Rana TM. Selective binding of TAR RNA by a Tat-derived beta-peptide. Org Lett. 2003; 5:3563–3565. [PubMed: 14507173]
40. www.hiv.lanl.gov
41. Futaki S, Nakase I, Suzuki T, Zhang, Sugiura Y. Translocation of Branched-Chain Arginine Peptides through Cell Membranes: Flexibility in the Spatial Disposition of Positive Charges in Membrane-Permeable Peptides. Biochemistry. 2002; 41:7925–7930. [PubMed: 12069581]

42. Park SH, Doh J, Park SI, Lim JY, Kim SM, Youn JI, Jin HT, Seo SH, Song MY, Sung SY, Kim M, Hwang SJ, Choi JM, Lee SK, Lee HY, Lim CL, Chung YJ, Yang D, Kim HN, Lee ZH, Choi KY, Jeun SS, Sung YC. Branched oligomerization of cell-permeable peptides markedly enhances the transduction efficiency of adenovirus into mesenchymal stem cells. Gene Ther. 2010; 17:1052–1061. [PubMed: 20485381]

43. Frankel AD, Pabo CO. Cellular uptake of the tat protein from human immunodeficiency virus. Cell. 1988; 55:1189–1193. [PubMed: 2849510]

44. Green M, Loewenstein PM. Autonomous functional domains of chemically synthesized human immunodeficiency virus tat trans-activator protein. Cell. 1988; 55:1179–1188. [PubMed: 2849509]

45. Torchilin VP. Tat peptide-mediated intracellular delivery of pharmaceutical nanocarriers. Adv Drug Del Rev. 2008; 60:548–558.

46. Milligan JF, Groebe DR, Witherell GW, Uhlenbeck OC. Oligoribonucleotide synthesis using T7 RNA polymerase and synthetic DNA templates. Nucleic Acids Res. 1987; 15:8783–8798. [PubMed: 3684574]

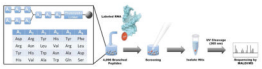

Figure 1.
High throughput screening of a branched peptide library with TAR RNA reveals peptide hits that are sequenced by MALDI-TOF.

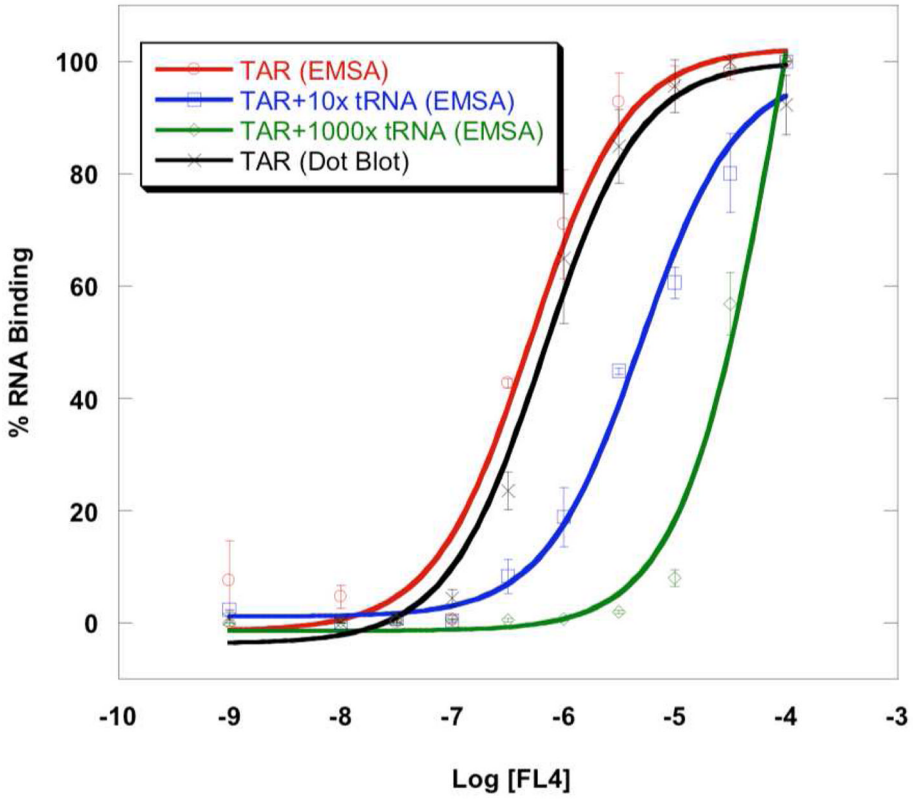

Figure 2.
Titration curves comparing EMSA and dot blot assay with or without competing tRNA.

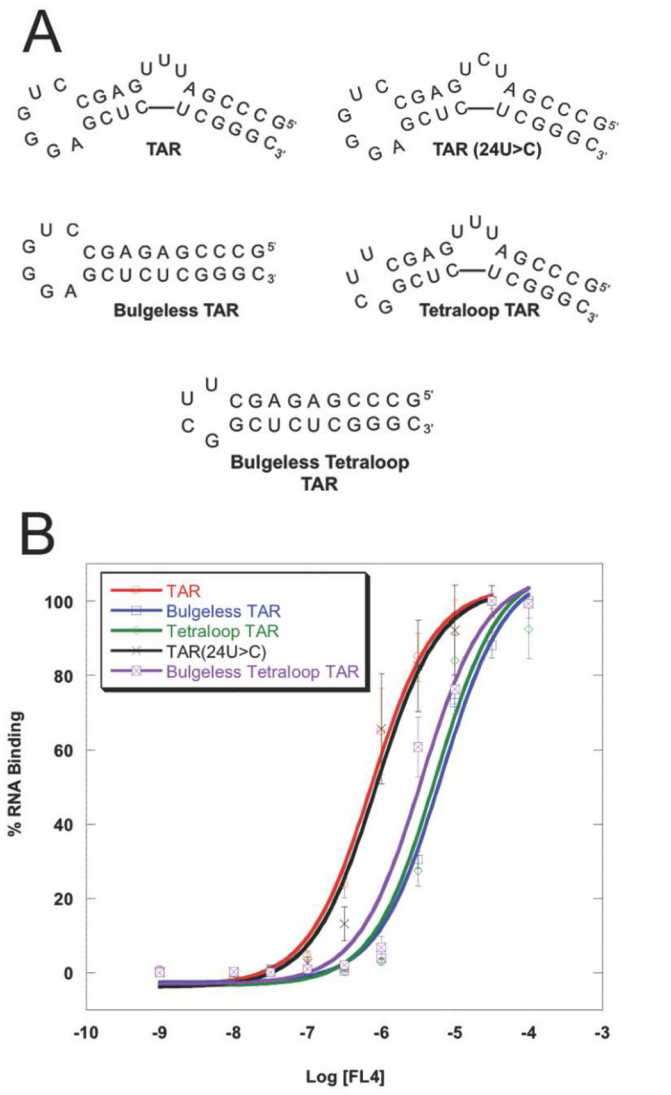

Figure 3.
Sequence and secondary structure of TAR RNA and variants (A) and titration curves of **FL4** with these RNAs (B).

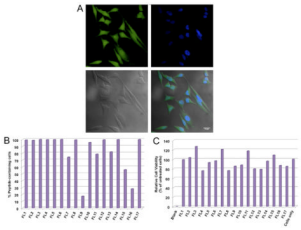

Figure 4.

A) Cellular uptake of branched peptides into HeLa cells, top left: fluorescence image of cells; top right: DAPI staining of the nucleus; bottom left: phase contrast image; bottom right: overlay of all images. White scale bar is 25μm. B) Cell permeability of FITC-labeled branched peptides by flow cytometry in HeLa cells. C). MTT cell toxicity assay.

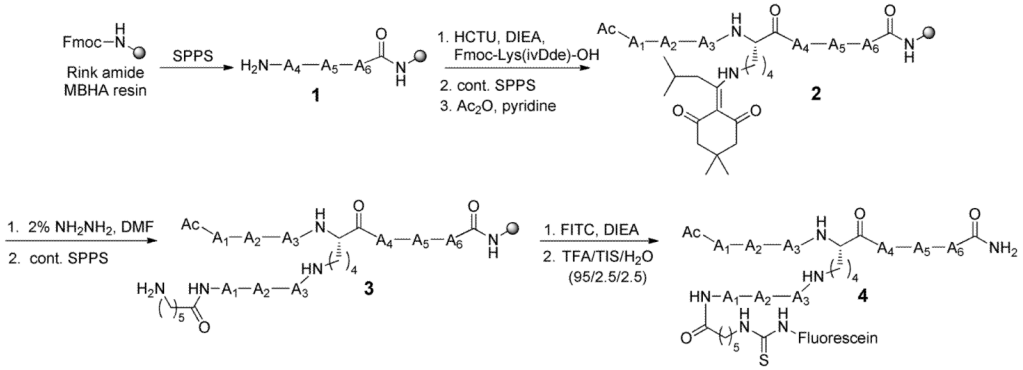

Scheme 1.
Synthesis of fluorescein-labeled branched peptides by solid-phase peptide synthesis (SPPS).

Table 1

Binding constants and molecular weights of hit BPs

Entry	Peptide	Sequence	K_d (μM)	MW (g/mol)
1	**FL4**	$(RRW)_2^*$ HAL	0.6 ± 0.1	1463.74
2	**FL6**	$(RRY)_2^*$ VRL	1.2 ± 0.2	1464.77
3	**FL7**	$(RRW)_2^*$ HYD	1.2 ± 0.2	1557.77
4	**FL12**	$(RRW)_2^*$ HAS	1.9 ± 0.3	1437.66
5	**FL5**	$(RRL)_2^*$ NRF	2.0 ± 0.3	1413.72
6	**FL1**	$(RRL)_2^*$ WYL	2.5 ± 0.3[a]	1458.80
7	**FL17**	$(RRL)_2^*$ HRF	3.1 ± 0.3	1436.76
8	**FL9**	$(RRA)_2^*$ NYF	3.7 ± 1.9	1336.55
9	**FL2**	$(YRA)_2^*$ HRF	7.5 ± 0.9	1366.58
10	**FL16**	$(RRL)_2^*$ HYL	7.7 ± 1.1	1409.73
11	**FL8**	$(YRL)_2^*$ WRL	7.8 ± 1.9[a]	1465.79
12	**FL11**	$(RRA)_2^*$ VYF	8.1 ± 1.3	1321.58
13	**FL3**	$(HRW)_2^*$ WAS	8.7 ± 3.1[a]	1448.64
14	**FL14**	$(RRY)_2^*$ VQL	20.2 ± 2.9	1436.71
15	**FL10**	$(DNL)_2^*$ HYF	NB[a]	1277.38
16	**FL13**	$(RRY)_2^*$ NQD	> 75	1453.61
17	**FL15**	$(RRA)_2^*$ VRD	> 75	1282.51
18	**T4-1**	RRWGHAL	> 75	
19(38)	**$Tat_{47–57}$**	GRKKRRQRRR	0.78	

[a] Performed with a final concentration of 5% DMSO. No binding observed (NB).

* = Lysine branching unit. Each value is an average of at least three experiments.